JBC ARTICLE

Using single-molecule FRET to probe the nucleotide-dependent conformational landscape of polymerase β-DNA complexes

Received for publication, February 14, 2020, and in revised form, May 7, 2020 Published, Papers in Press, May 8, 2020, DOI 10.1074/jbc.RA120.013049

Carel Fijen[1,2,*], **Mariam M. Mahmoud**[2], **Meike Kronenberg**[1], **Rebecca Kaup**[1], **Mattia Fontana**[1], **Jamie B. Towle-Weicksel**[2], **Joann B. Sweasy**[2], **and Johannes Hohlbein**[1,3,*]

From the [1]*Laboratory of Biophysics, Wageningen University & Research, Wageningen, The Netherlands,* [2]*Department of Therapeutic Radiology, Yale University School of Medicine, New Haven, Connecticut, USA, and* [3]*Microspectroscopy Research Facility, Wageningen University & Research, Wageningen, The Netherlands*

Edited by Patrick Sung

Eukaryotic DNA polymerase β (Pol β) plays an important role in cellular DNA repair, as it fills short gaps in dsDNA that result from removal of damaged bases. Since defects in DNA repair may lead to cancer and genetic instabilities, Pol β has been extensively studied, especially its mechanisms for substrate binding and a fidelity-related conformational change referred to as "fingers closing." Here, we applied single-molecule FRET to measure distance changes associated with DNA binding and prechemistry fingers movement of human Pol β. First, using a doubly labeled DNA construct, we show that Pol β bends the gapped DNA substrate less than indicated by previously reported crystal structures. Second, using acceptor-labeled Pol β and donor-labeled DNA, we visualized dynamic fingers closing in single Pol β-DNA complexes upon addition of complementary nucleotides and derived rates of conformational changes. We further found that, while incorrect nucleotides are quickly rejected, they nonetheless stabilize the polymerase-DNA complex, suggesting that Pol β, when bound to a lesion, has a strong commitment to nucleotide incorporation and thus repair. In summary, the observation and quantification of fingers movement in human Pol β reported here provide new insights into the delicate mechanisms of prechemistry nucleotide selection.

DNA repair is pivotal for maintaining genome integrity (1). Among the most common damages of DNA are base lesions, in which the chemical structure of a single base has been altered (2, 3). These modifications may disturb proper base pairing and can lead to harmful mutations in the genome. In eukaryotes, the base excision repair (BER) pathway is responsible for replacing these damaged bases (4, 5). Within BER, the damaged base(s) and the corresponding part of the backbone are removed, creating a gap of one or more bases in the DNA (6). DNA polymerase β (Pol β) then binds to the gap and subsequently fills the gap by adding cognate nucleotides to the 3′ end of the primer strand (7, 8).

Pol β is one of the smallest eukaryotic polymerases and belongs to the X-family of DNA polymerases (9). Pol β consists of a polymerase domain and a lyase domain (10) and was shown to adopt an elongated structure in solution (11, 12). Upon binding to gapped DNA, the lyase domain interacts with the 5′ phosphate on the downstream strand, while the polymerase domain adopts a structure that has been compared with a hand (10). Crystal structures have suggested that Pol β bends its DNA substrate with an angle of ∼90° (13). Incoming nucleotides then bind to a subdomain known as the "fingers," forming the ternary complex. A conformational change called "fingers closing" positions the nucleotide closer to the active site to facilitate chemistry. Studies on *Escherichia coli* DNA polymerase I (KF), which undergoes a very similar conformational change from an open to a closed conformation, suggested that the fingers do not close entirely when a noncomplementary nucleotide is bound. Instead, an intermediate "ajar" conformation was identified, which serves as a fidelity checkpoint (14–16). At the same time, incorrect nucleotides were found to promote dissociation of KF from the DNA (17, 18).

In any cell, noncomplementary nucleotides and ribonucleotides vastly outnumber correct nucleotides. In cancerous cells, the nucleotide concentrations increase further (19), highlighting that effective mechanisms for discriminating correct from noncomplementary nucleotides are pivotal for faithful DNA repair. However, the existence of a fidelity checkpoint during fingers closing is not widely accepted for Pol β. An early study using small-angle X-ray scattering suggested that mismatched ternary complexes exist in a partially closed state (20). In contrast, several later crystal structures with mismatched nucleotides or their nonhydrolyzable analogues showed that the fingers domain adopts an overall closed conformation, although the active site is distorted (21–23). Fidelity-reducing manganese was necessary to stabilize these mismatched complexes. Studies in presence of physiological magnesium underscore the difficulty for Pol β to form stable closed complexes with incorrect nucleotides (24, 25). The presence and nature of a partially closed fingers conformation as a fidelity checkpoint in Pol β therefore remain unknown. Interestingly, the Pol β mutator variant I260Q has recently been reported to exhibit a collapsed fingers domain in the binary complex (26), suggesting that positioning of the fingers domain is important for Pol β fidelity.

This article contains supporting information.

* For correspondence: Carel Fijen, carelfijen89@gmail.com; Johannes Hohlbein, johannes.hohlbein@wur.nl.

Present address for Jamie B. Towle-Weicksel: Physical Sciences Department, Rhode Island College, Providence, Rhode Island, USA.

Present address for Joann B. Sweasy: University of Arizona Cancer Center, University of Arizona, Tucson, Arizona, USA.

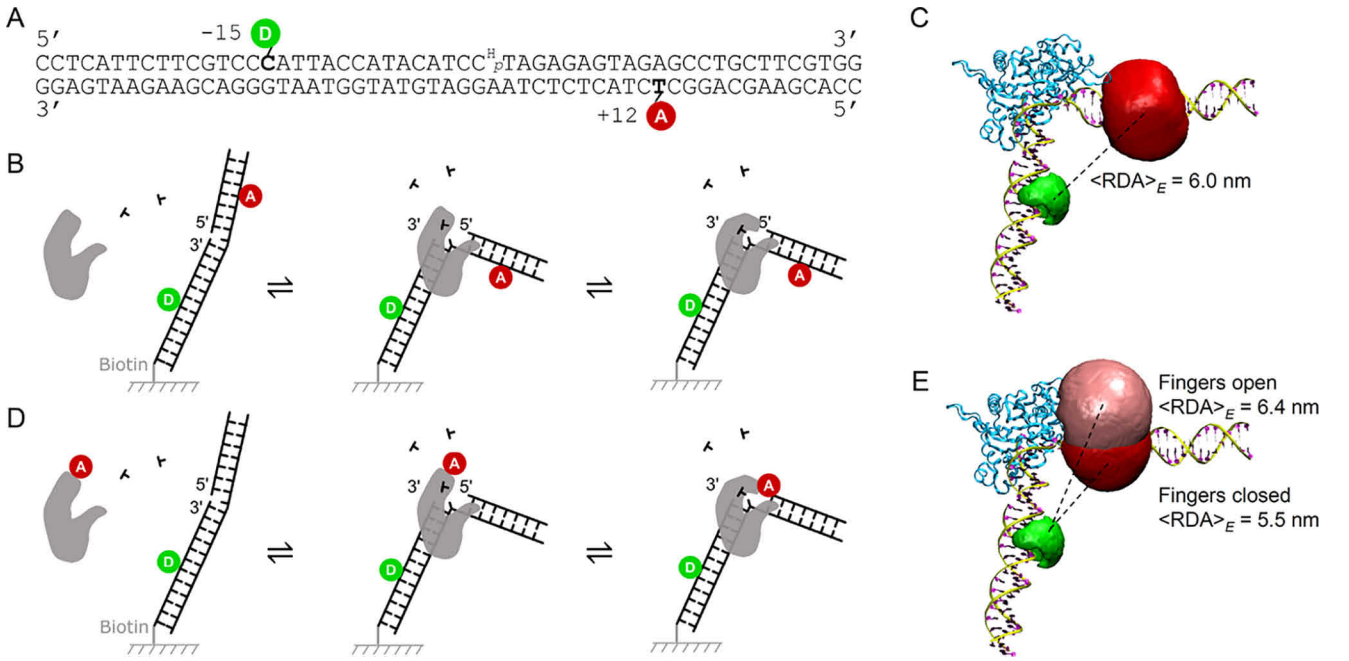

Figure 1. Experimental design. *A*, sequence and labeling positions of the gapped DNA construct. The 3′ end of the primer is dideoxy-terminated, and a phosphate group is present at the 5′ end of the complementary strand. *B*, schematic overview of the assay with the bending sensor. A gapped DNA substrate is thought to bend upon binding of Pol *β*, which translates to a change in FRET efficiency. *C*, extended crystal structure (PDB entry 1BPX). Accessible volumes of Cy3B (*green*) and Cy5 (*red*) are outside the putative binding region of the polymerase. *D*, schematic overview of the fingers closing assay. Pol *β*, labeled with Alexa Fluor 647 on the fingers domain, binds to a gapped DNA substrate that is labeled with Cy3B. Fingers movement results in a change in FRET efficiency. *E*, structure 1BPX with the accessible volumes of Alexa Fluor 647, in the open (*pink*) and closed (*red*) conformations. (The accessible volume of the closed conformation was modelled using structure 1BPY, which is not shown here). Cy3B is on the primer. The distance between the donor and acceptor dyes decreases with fingers closing.

To study fingers movement of Pol *β* in more detail, Towle-Weicksel *et al.* introduced an assay based on ensemble FRET to monitor fingers closing using stopped-flow experiments (24). This approach used Pol *β* labeled with a fluorophore on the fingers subdomain (at position V303C) and DNA substrates labeled with a quencher. By fitting the stopped-flow traces to a multistep kinetic model, the authors extracted rates for fingers closing and opening in presence of the complementary nucleotide. Noncomplementary nucleotides were not found to induce fingers closing, leading the authors to hypothesize that discrimination between correct and incorrect nucleotides already takes place before fingers closing. In later work, the authors showed that a low-fidelity Pol *β* mutant found in cancer cells exhibits altered fingers dynamics (25).

Here, we developed two single-molecule assays to study the DNA binding behavior and fingers movement of Pol *β*, for which we used a combination of FRET and total internal reflection fluorescence (TIRF) microscopy in order to monitor hundreds of molecules in parallel and in real time. The first assay uses a doubly labeled gapped DNA substrate to report on binding of unlabeled WT Pol *β*. We found that strong DNA bending upon binding of Pol *β*, as suggested by several crystal structures, is not the dominant binding mode. A second assay, inspired by various single-molecule studies on *E. coli* DNA polymerase I (KF) (16, 18, 27), employs a similar design as the stopped-flow experiments discussed above; the fingers subdomain of Pol *β* is labeled with an acceptor fluorophore, whereas a gapped, nonextendable DNA substrate bears the donor fluorophore. The labeling position on the DNA was chosen such that open and closed conformations of the fingers exhibit different FRET efficiencies (*E*) when Pol *β* is bound to the surface-immobilized DNA substrate. This approach allowed us to visualize fingers movement of individual Pol *β* molecules repeatedly in response to either complementary or noncomplementary nucleotides that were added to the buffer. We found that correct nucleotides induce fingers closing; incorrect nucleotides, on the other hand, are quickly rejected by the fingers domain. Contrary to the destabilization of polymerase-DNA complexes that was observed for KF, Pol *β* binds more tightly to the DNA in the presence of incorrect nucleotides. This suggests that in BER quick repair may be more important than an additional fidelity mechanism.

Results

A doubly labeled gapped DNA sensor indicates binding of Pol β

First, we assessed binding of WT Pol *β* to dsDNA with a 1-nucleotide gap, mimicking the BER pathway intermediate that is the natural and preferred substrate of Pol *β* (Fig. 1, *A–C*) (10). Crystal structures 1BPX and 1BPY suggested that the DNA adopts a sharply bent conformation (~90°) after binding of Pol *β*. We set out to make bending a direct indicator for polymerase binding. To this end, we labeled our DNA substrate with a donor dye on the primer and an acceptor dye on the template, at positions that are outside the putative binding region of the polymerase (as judged from crystal structures 1BPX and 1BPY), thus creating a "bending sensor."

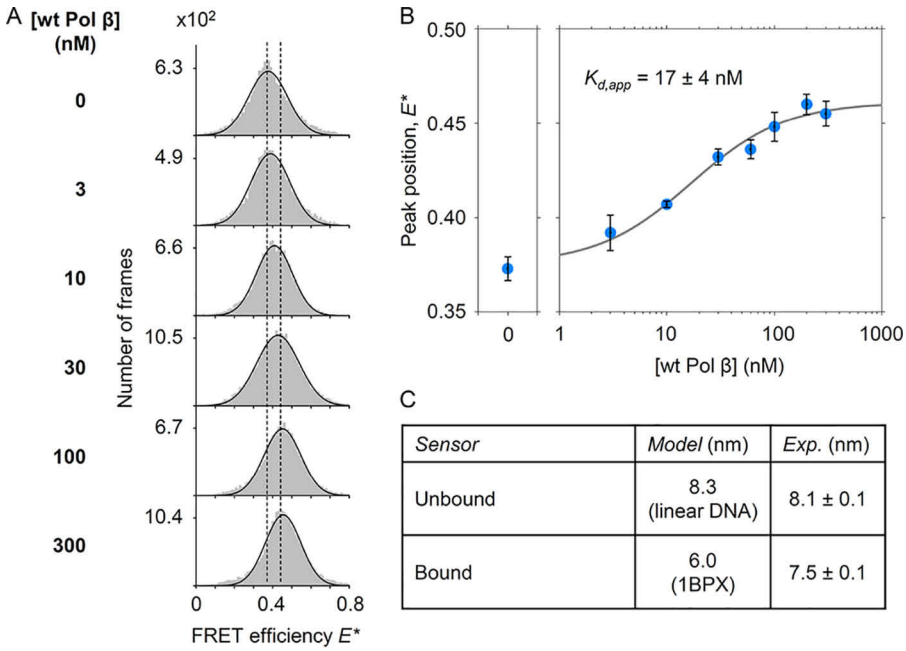

C

Sensor	*Model* (nm)	*Exp.* (nm)
Unbound	8.3 (linear DNA)	8.1 ± 0.1
Bound	6.0 (1BPX)	7.5 ± 0.1

Figure 2. Response of the gapped DNA bending sensor to WT Pol β. *A*, the mean uncorrected FRET efficiency *E** increases with increasing concentrations of WT Pol *β*. *B*, mean FRET efficiencies from *A* were plotted against WT Pol *β* concentration. A fit to a binding isotherm (*gray line*) reveals a $K_{d,app}$ of 17 ± 4 nM. See Table S2 for the correction procedure. Each data point represents the mean of three independent experiments. Error bars indicate the S.E. *C*, modelled and experimentally determined inter-fluorophore distances of both the native bending sensor and the bent conformation are shown. Each experimental value represents the mean of triplicate measurements.

In the absence of DNA polymerases, we found an apparent FRET efficiency *E** of 0.37 (Fig. 2*A*), corresponding to an inter-fluorophore distance of 8.1 ± 0.1 nm (mean ± S.E.) after corrections (see Table S2 and Refs. 28 and 29 for a detailed discussion of the correction procedure). A standard B-DNA model of a nongapped construct predicted an inter-dye distance $<RDA>_E$ of 8.3 nm. This value represents the maximum possible distance between the fluorophores (i.e. in the absence of any bending); the slightly lower inter-dye distance for the unbound bending sensor is consistent with the fact that adding the gap in the DNA structure introduces more flexibility and the possibility of visiting bended conformations even in the absence of protein binding.

We then tested our sensor with *E. coli* DNA polymerase I (KF), which was shown to bend gapped DNA (30). Indeed, with increasing concentrations of this polymerase, a second peak at high FRET efficiency emerged (Fig. S1). For Pol *β*, however, we observed not a second FRET peak but rather an unexpected peak shift. Because of our use of alternating-laser excitation (ALEX) (28, 31), in which direct excitation of the donor is alternated with the direct excitation of the acceptor fluorophore to report on the photophysical state of the acceptor, we were able to rule out the possibility that this peak shift was due to protein-induced fluorescence enhancement (32, 33). This means that the change in FRET efficiency must be solely due to a distance change and not to interactions between the protein and the dyes (see Fig. S2 for full *E**/S histograms and a single-molecule time trace; also see Table S2). We confirmed the formation of Pol *β*-DNA complexes by EMSA (Fig. S3), which suggested that DNA binding takes place at Pol *β* concentrations as low as 1 nM, thereby confirming previously reported values in the low nanomolar range (25, 34). We then fitted the peak shift in our FRET efficiency histograms using a binding isotherm, introducing an apparent binding constant, $K_{d,app}$, which indicates the Pol *β* concentration at which the magnitude of the bend appears to be 50% (Fig. 2*B*). We obtained a $K_{d,app}$ value of 17 ± 4 nM (Fig. 2*B*) and a FRET efficiency that levels off at *E** = 0.46, corresponding to an inter-fluorophore distance of 7.5 nm after corrections (Fig. 2*C* and Table S2). This distance suggests that the bend measured here is less sharp than the bend seen in the crystal structure.

Singly labeled Pol β reveals fingers closing in the presence of the correct nucleotide

Next, we studied the ability of fluorescently labeled Pol *β* to report on the conformation of the fingers subdomain (Fig. 1, *D* and *E*). Reasoning that the different labeling positions may have an influence on the K_d, we first measured binding of the labeled polymerase to the singly labeled DNA construct by recording time traces at increasing concentrations of Pol *β*. We identified binding events and constructed dwell time histograms to obtain k_{off} and k_{on} (Fig. S4). Although nonspecific adsorption made measuring at concentrations higher than 50 nM impossible, we inferred that the K_d must be around 100 nM. This value represents an upper limit, since it does not take into account the labeling efficiency (60–70%; see "Experimental Procedures") and acceptor photobleaching. Additionally, we found that ~6% of all binding events involved two acceptors, with this number being independent of the protein concentration in the range that we measured. We assume that these are doubly labeled proteins, since cysteine 178 (although buried) is still in place in this version of the polymerase and could have been labeled with

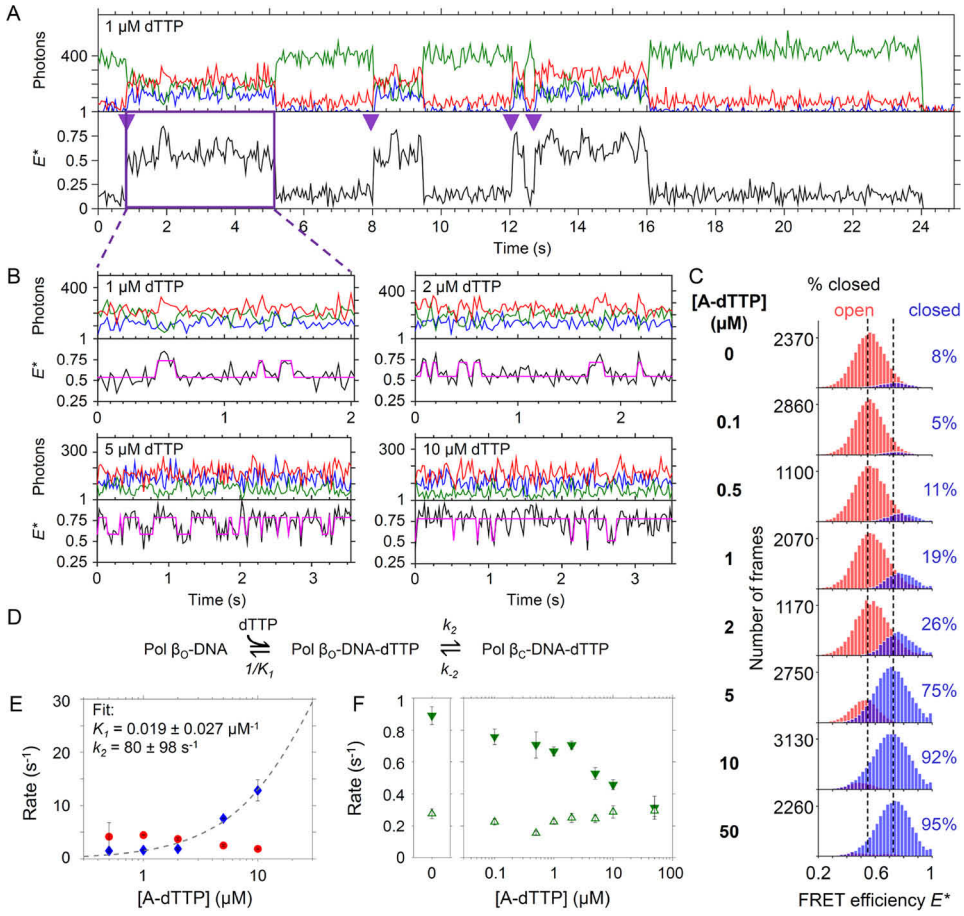

Figure 3. Fingers opening and closing of Pol β revealed by single-molecule FRET. *A*, time trace of a single DNA molecule in the presence of 10 nM labeled Pol β and 1 μM complementary dTTPs. Pol β binding events are indicated with *inverted purple triangles*. At $t = 24$ s, the donor bleaches. *B*, time traces of labeled Pol β-DNA complexes, at various concentrations of dTTP. The first trace ([dTTP] = 1 μM) is a binding event taken from *A*. FRET efficiency *E** (*black trace*) is calculated from the *DD* signal (*green trace*) and the *DA* signal (*red trace*) in the *upper panel*. The *AA* signal (*blue trace*) is shown here as well, to indicate that the observed events are not due to acceptor photophysics. An HMM fit (*magenta*) indicates the open and closed conformation of the fingers. *C*, corresponding FRET efficiency histograms (32 bins between $E^* = 0.2$ and $E^* = 1$) of the Pol β-DNA complexes. The FRET efficiencies of the open (*red*) and closed (*blue*) conformations were plotted after the states had been assigned via HMM. *D*, schematic model used to describe the dynamics of fingers movement. *E*, observed closing rates $k_{close,obs}$ (*blue diamonds*) and opening rates k_{open} (*red circles*) plotted against [dTTP]. Data were fit to a function described in the main text (*dashed line*) and derived from the model depicted in *D*. Error bars represent the 95% confidence intervals obtained from fitting the dwell times (see Fig. S5 for dwell time histograms). *F*, rates k_{on} (*green open triangles*) and k_{off} (*green solid inverted triangles*) plotted against [dTTP]. Complementary dTTPs stabilize the Pol β-DNA complex. k_{off} decreases with increasing concentrations of dTTP, while k_{on} remains constant. Error bars represent the 95% confidence intervals obtained from fitting the dwell times (see Fig. S5 for dwell time histograms).

very low efficiency. This is further supported by the observation that the two acceptors almost always appeared together in the single-molecule time traces.

To measure fingers closing, we decided to use a Pol β concentration of 10 nM. Although far lower than the K_d, we preferred this concentration since it resulted in very low nonspecific adsorption while giving a reasonable number of binding events. We performed a titration of Pol β with increasing concentrations of the complementary nucleotide dTTP opposite template A (i.e., A-dTTP). Time traces of single, donor-labeled DNA showed binding events of single, acceptor-labeled Pol β as an increase in the acceptor emission after acceptor excitation (*AA*) and the appearance of FRET (Fig. 3*A*). Hidden Markov modelling (HMM) was used to identify the open (low *E**) and closed (high *E**) conformations within time traces of individual binding events (Fig. 3*B*). At a dTTP concentration of 1 μM, traces predominantly show low FRET efficiency, with only brief excursions to the high FRET efficiency that is associated with closed fingers. At higher dTTP concentrations, longer residence times in the closed state are observed. We constructed FRET efficiency histograms and indicated the open and closed populations, as determined by HMM (Fig. 3*C*). In the absence of dTTPs, the fingers mostly adopt the open conformation (92%). With increasing dTTP concentration, the closed conformation is increasingly populated. At a dTTP concentration of 50 μM, the fingers are mostly closed (95%).

Using accurate FRET, we determined the distances associated with open and closed fingers (Table S3). We found interfluorophore distances of 6.5 ± 0.0 (0.047) nm for the open and 5.7 ± 0.1 nm for the closed conformation. These distances are in excellent agreement with the distances of 6.4 nm and 5.5 nm predicted from structural modelling with the FPS software (see "Experimental Procedures"). We note that the less sharp bend observed in our DNA substrate does not appear to alter the distance between the fingers domain and the primer.

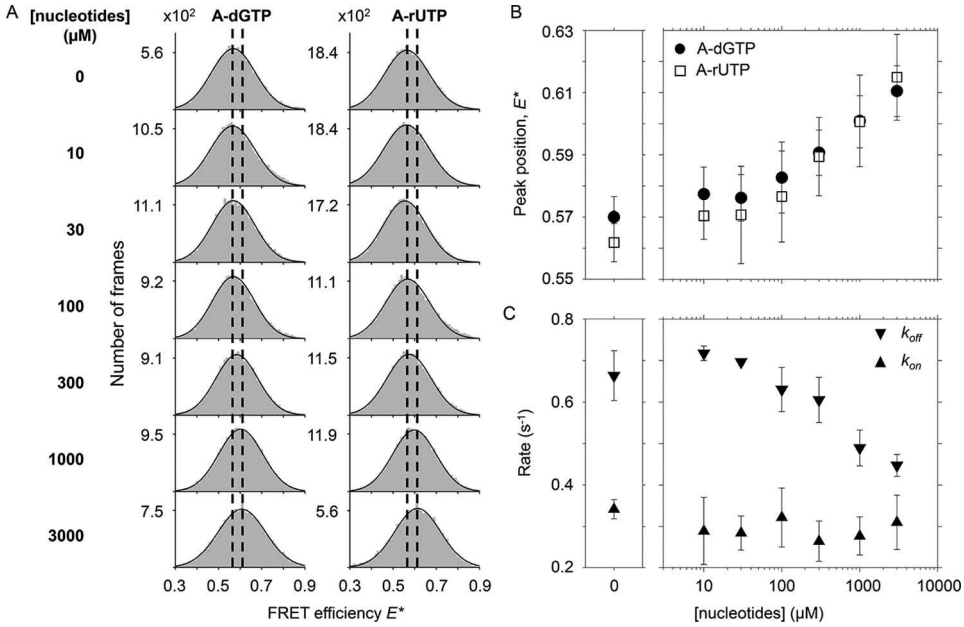

Figure 4. Incorrect dNTPs are quickly rejected but stabilize the polymerase-DNA complex. *A*, FRET efficiency histograms of Pol β-DNA complexes at increasing [dGTP] and [rUTP]. Histograms were obtained by calculating FRET efficiencies from polymerase binding events identified in time traces. Dashed lines are added for visual guidance. *B*, position of the main peak plotted against [nucleotides]. Both dGTPs and rUTPs cause a shift in the peak of the open conformation. Each data point represents the mean of three independent experiments (Table S4). Error bars indicate the S.E. *C*, rates k_{on} and k_{off} at increasing concentrations of dGTPs. k_{off} decreases with increasing concentrations of dNTPs, while k_{on} remains constant. Each data point represents the mean of three independent experiments (see Fig. S6 for dwell time histograms). *Error bars* indicate the S.E.

Dwell time histograms of the open and closed conformations were constructed and fitted with exponential decay curves (Fig. S5). The rate of fingers closing is extracted from the dwell times in the open conformation, while the rate of fingers opening is extracted from the dwell times in the closed conformation. Plotting $k_{obs,close}$ and k_{open} against the concentration of dTTP showed that the closing rate is concentration dependent whereas the opening rate remains largely constant, with a slight decrease that we attribute to missed events at higher concentrations of dTTP.

A model that links fingers closing to the affinity of complementary nucleotides without accounting for fingers closing in the binary complex was previously described and applied to stopped-flow data (Fig. 3*D*) (24, 25). In our data, the rare fingers closing in the binary complex (measured at a dTTP concentration of 0 μM) did not allow us to construct a suitable dwell time histogram even though we analyzed more than 1000 binding events. We adapted the model to exclude any steps after fingers closing, as the use of dideoxy-terminated primer DNA prevents the incorporation of nucleotides. Thus, the concentration of dTTPs relates to $k_{obs,close}$ as follows:

$$k_{obs,close} = \frac{K_1 k_2 [dTTP]}{1 + [dTTP] K_1}$$

in which K_1 is the association constant for dTTPs and k_2 is the closing rate with dTTP bound to the fingers. We fitted our data with no constraints for K_1 and k_2 (Fig. 3*E*) and found a k_2 of 80 ± 98 s^{-1} (mean ± S.E.) and a K_1 of 0.019 ± 0.027 μM^{-1} (corresponding to a $K_{d(dTTP)}$ of 53 μM). The large errors are due to experimental constraints such as the limited acquisition rate of the camera (40 s^{-1}). At dTTP concentrations higher than 10 μM, the lifetime of the open conformation is often too short to be clearly resolved; similarly, lifetimes of the closed state shorter than 50 ms are difficult to resolve.

We noted that the duration of Pol β-DNA binding events increased with increasing dTTP concentrations by observing a decrease in k_{off}, while k_{on} was not affected (Fig. 3*F*). This finding indicates that complementary nucleotides stabilize the polymerase-DNA complex.

The fingers domain quickly rejects incorrect dGTPs and rUTPs

Previous work with DNA polymerase I (KF) has shown that increasing concentrations of an incorrect nucleotide shift the position of the fingers open peak toward a slightly higher FRET efficiency, likely caused by the polymerase quickly screening and rejecting incorrect nucleotides (15, 18). This shift in FRET efficiency has been linked to the existence of a partially closed conformation of the fingers for DNA polymerase I. To investigate the potential existence of a similar conformation in Pol β, we studied the positioning of the fingers in the presence of increasing concentrations of incorrect dGTPs and rUTPs. Binding events were identified in the single-molecule time traces and used to construct FRET efficiency histograms (Fig. 4, *A* and *B*). Indeed, the previously identified high FRET state as seen for complementary dTTPs is not present; instead, a shift in E^* from ~0.56 to ~0.61 is observed, reminiscent of what has been shown for DNA polymerase I (KF). We note that neither the FRET efficiency distributions nor the single-molecule time traces show two separate states. We attribute this to temporal averaging; the conformational changes occur faster than the acquisition rate of our camera (40 s^{-1}), preventing us from directly detecting transitions from the open to a closed or partially closed

state, even when using the HMM of ebFRET. It should be noted that these transitions were also not directly detectable for doubly labeled DNA polymerase I (KF) in the work of Evans *et al.*, for which a higher time resolution was used (100 s^{-1}) (18).

Next, we asked whether incorrect nucleotides have an influence on the stability of the polymerase-DNA complex. Markiewicz *et al.* and Evans *et al.* showed, that for DNA polymerase I (KF), noncomplementary dGTPs increase k_{off} (17, 18). We used all polymerase binding events in our time traces to construct dwell time histograms (Fig. S5). Fitting with an exponential decay function yielded values for k_{on} and k_{off} for every nucleotide concentration of the titration series (Fig. 4*C*). Interestingly, k_{off} decreases slowly with increasing dGTP concentrations, mimicking the trend seen for correct dTTPs. This indicates that for Pol β bound to gapped DNA even incorrect nucleotides stabilize the polymerase-DNA complex, albeit at higher concentrations than the correct dNTP.

Discussion

The use of single-molecule FRET allowed us to observe and analyze conformational changes of individual Pol β-DNA complexes in real time, thereby overcoming some of the ensemble averaging inherent to conventional fluorescence-based techniques, such as stopped-flow experiments.

Our experiments with WT Pol β showed substrate binding with an apparent K_d of 17 ± 4 nM. Gel mobility shift assays, as performed by us and others, also resulted in values in the low nanomolar range (25), while a titration based on single-turnover analysis at different DNA concentrations revealed a K_d of 22 nM (34). Our distance measurements on the bending sensor, however, revealed that DNA bending upon polymerase binding occurs to a smaller extent than predicted by various structures resolved with X-ray crystallography. The inter-fluorophore distances that we calculated for the fingers conformational change (between residue V303C and the primer) are consistent with crystal structures 1BPX and 1BPY, implying that it is the flexible positioning of the downstream strand that determines the bend.

We further studied the conformational change associated with fingers closing using fluorescently labeled Pol β. We observed an increase in the rate of fingers closing with increasing concentrations of the complementary dNTP, as expected for an induced fit mechanism. Previous studies in Pol β (24, 25) found a rapid fingers closing rate of 98 s^{-1}, close to the maximum rate of 80 s^{-1} that we determined from our fit. Additionally, we showed that polymerase-DNA complexes become more stable with increasing dTTP concentrations, due to a decrease in k_{off}. The K_d of the incoming correct nucleotide ($1/K_1$ = 53 μM for dTTP) is higher than that determined before using chemical quench analysis (K_d = 2.5 μM) (24, 25). We note that the K_d as defined in our model represents the dNTP concentration at which the fingers closing rate is at half-maximum, whereas the K_d as defined using chemical quench analysis includes a fast chemistry step that is likely preventing nucleotide binding from reaching the equilibrium, as illustrated by Kellinger and Johnson (35).

We found a small increase in FRET efficiency of the fingers when supplying noncomplementary nucleotides. We were initially tempted to attribute this increase to formation of a partially closed fingers conformation. However, we are cautious of doing so, since the existence of such a conformation has been challenging to show using single-molecule techniques. An early study on DNA polymerase I (KF), using a single label on the protein and a single label on the DNA, showed ternary complexes in a state with a FRET efficiency between open and closed fingers in single-molecule time traces (16). The time resolution of these traces was 100 ms, suggesting that the ajar conformation is stable on this time scale and that rejection of incorrect nucleotides is therefore relatively slow. Another study on the same polymerase used a design with both fluorophores on the enzyme (18). That study revealed an increase in FRET efficiency very similar to what we observe, being visible on the population level but not in individual traces (which were acquired at 10-ms resolution). The authors attributed this increase in FRET efficiency to an ajar conformation of the fingers domain, reasoning that a rapid rejection mechanism for incorrect nucleotides prevented them from observing the conformation directly in their single-molecule time traces. Fast rejection is indeed necessary to reach the expected DNA polymerase I synthesis rate of ~15 nucleotides per second (36).

Even though we cannot directly detect an ajar conformation in our Pol β time traces, we can draw important conclusions about the underlying fidelity mechanism of the enzyme. Like DNA polymerase I (KF), Pol β rejects incorrect nucleotides faster than the acquisition rate of the camera (40 s^{-1}). This is much faster than fingers opening in the presence of correct dTTPs, which we were able to measure directly at ~4 s^{-1}. Thus, even though increasing concentrations of incorrect nucleotides will drive the equilibrium toward a closed (or partially closed) state of the fingers, these excursions are always short. With our limited time resolution, temporal averaging of these events leaves individual excursions irresolvable but results in a slight overall increase in FRET efficiency. Despite the fast rejection rate, we showed that noncomplementary nucleotides stabilize the Pol β-DNA complex, similar to the effect seen for correct dTTPs. Apparently, the presence of both correct and incorrect nucleotides can enhance binding to a gapped DNA substrate up to at least 2-fold by decreasing k_{off}. Interestingly, this is fundamentally different from the destabilizing effect observed for incorrect nucleotides with DNA polymerase I (KF) (17, 18). We note that, for Pol β, stabilization is in accordance with a linear reaction pathway, as illustrated in Fig. 3*D*, and an increase in dNTPs, correct or incorrect, will shift the equilibrium to the right (and make incorporation more favorable). For DNA polymerase I (KF), the pathway is apparently not linear; incorrect nucleotides not only lead to fast rejection but also can lead to disassembly of the entire ternary complex (17, 18). Although we do not know at exactly what stage in the reaction path this disassembly happens, it is a mechanism that Pol β does not seem to possess. Given its role to quickly repair damaged DNA in the BER pathway, however, stable gap binding as well as incorporation of an incorrect nucleotide may be more beneficial for Pol β than an additional fidelity mechanism. It will be interesting to see in follow-up single-molecule studies how the balance between fingers closing and reopening is

affected in mutator variants of Pol β, similar to what has been done for DNA polymerase I (KF) (15).

In conclusion, the direct observation of fingers movement allowed us to obtain conformational rates that describe the dynamic equilibria of individual ternary complexes under pre-chemistry conditions, shining light on the mechanism of nucleotide selection by Pol β. Future experiments, ideally complemented by using doubly labeled Pol β, will further help elucidate the dynamic-structural relations between DNA, (mutator) Pol β, and other enzymes of the BER.

Experimental procedures

Polymerase purification and labeling

Here we use the term WT Pol β to refer to Pol β bearing the substitutions C239S, C267S, and V303C, introduced to have a single cysteine residue on the fingers subdomain that can react with the fluorophore bearing a maleimide moiety (24). For the assays in which the fingers conformational change was studied, the V303C was labeled with Alexa Fluor 647 following procedures described before (24). The labeling efficiency was 60–70%, as determined by absorbance measurements (data not shown). For experiments with *E. coli* DNA polymerase I (KF), we used the D424A mutant, which abolishes the 3′ to 5′ exonuclease activity.

DNA substrate design

As a first step to construct a gapped DNA construct labeled at adequate positions with fluorophores, we examined crystal structures 1BPX and 1BPY (13), which represent Pol β bound to gapped DNA with open and closed fingers, respectively. We extended the DNA from the crystal structures on both sides of the polymerase with a B-DNA helix, using the 3D-DART server (37). Next, we used FPS (short for FRET-restrained positioning and screening) software to model the accessible volumes of the fluorophores at potential labeling positions on the DNA and the determine inter-dye distances $<RDA>_E$ (38). Modelling parameters include the dimensions of the fluorophore and the dimensions of the linker (Table S1). We selected two labeling positions (positions −15 and +12; see Fig. 1, *A–C*) that are located outside the binding region of Pol β. Using Cy3B as a donor fluorophore at the −15 position and Cy5 as an acceptor at position +12, these positions are within the distance range for FRET ($R_{0,Cy3B\rightarrow Cy5}$ = 6.9 nm, $<RDA>_{E,model}$ = 6.0 nm). Additionally, the Cy3B at the −15 position is close enough to the fingers subdomain to exhibit FRET with the Alexa Fluor 647 ($R_{0,Cy3B\rightarrow Alexa\ Fluor\ 647}$ = 6.9 nm, $<RDA>_{E,fingers\ open}$ = 6.4 nm, $<RDA>_{E,fingers\ closed}$ = 5.5 nm) (Fig. 1, *D* and *E*). Importantly, these distances translate to a large difference in FRET efficiency (*E*) between the open (*E* = 0.60) and closed (*E* = 0.79) conformations of the fingers.

We annealed the 1-nucleotide gapped DNA complex using template A from a 30-mer dideoxy-terminated primer sequence (biotin-5′-CCT CAT TCT TCG TCC CAT TAC CAT ACA TCC_H-3′), a 55-mer template sequence (5′-CCA CGA AGC AGG CTC TAC TCT CTA AGG ATG TAT GGT AAT GGG ACG AAG AAT GAG G-3′), and a 24-mer downstream complementary strand (5′-phosphate-TAG AGA GTA GAG CCT GCT TCG TGG-3′), which we ordered from IBA Life Sciences (Germany) and Eurogentec (Belgium). All oligonucleotides were HPLC or gel purified prior to use. The dideoxy-terminated primer prevents incorporation of the nucleotide, allowing us to study only the prechemistry steps. The primer sequence was internally labeled with donor dye Cy3B through a C6 linker at the previously determined −15 cytosine base; for experiments with unlabeled WT Pol β, also the template was internally labeled with Cy5 through a C6 linker at the +12 thymine base.

EMSAs

^{32}P-labeled gapped DNA (0.1 nM, the same sequence as the bending sensor) was mixed with a range of WT Pol β concentrations (0 or 0.06–500 nM) in a buffer containing 10 mM Tris-HCl, pH 7.6, 6 mM $MgCl_2$, 100 mM NaCl, 10% glycerol, and 0.1% IGEPAL (a nonionic, nondenaturing detergent). Samples were loaded on 6% native polyacrylamide gels, which were run at 150 V for 3 h. The shift was imaged on a phosphor screen.

TIRF experiments

Labeled DNA molecules were immobilized on PEGylated glass coverslips using a protocol described before (18). We used flow channels formed by Ibidi sticky-Slides $VI^{0.4}$. Molecules were imaged on a home-built TIRF microscope, described in more detail elsewhere (39). All experiments were performed using ALEX, in which the direct excitation of the donor alternates with the direct excitation of the acceptor fluorophore (28, 31). Experiments on WT Pol β and doubly labeled DNA were performed with laser powers of 1.5 mW (λ = 561 nm) and 1.5 mW (λ = 638 nm). The excitation time and camera frame time were set to 50 ms. Raw FRET efficiency (E^*) was calculated using $E^* = DA/(DD + DA)$, in which *DD* is donor emission intensity after donor excitation and *DA* is acceptor emission intensity after donor excitation (FRET). Acceptor emission intensity after acceptor excitation, *AA*, as obtained during ALEX, was used for time trace selection. Experiments with fluorescently labeled Pol β were performed with laser powers of 1.5 mW (λ = 561 nm) and 0.75 mW (λ = 638 nm). The excitation time and frame time were 25 ms. Surface-immobilized DNA molecules were imaged in a buffer containing either WT Pol β (3, 10, 30, 60, 100, 200, and 300 nM) or labeled Pol β-V303C-Alexa Fluor 647 (10 nM in experiments with dTTPs, 20 nM in experiments with dGTPs and rUTPs). Imaging buffer further contained 50 mM Tris, pH 7.5, 10 mM $MgCl_2$, 100 mM NaCl, 100 μg/ml BSA, 5% glycerol, 1 mM DTT, 1 mM Trolox, 1% gloxy, and 1% glucose. Experiments conducted without NaCl are marked in the text. Trolox is a triplet state quencher (40); gloxy and glucose form an enzymatic oxygen scavenger system to prevent premature fluorophore bleaching (41). When specified, complementary dTTPs were added to achieve final concentrations of 0.1, 0.5, 1, 2, 5, 10, and 50 μM; concentrations of incorrect dGTPs and rUTPs were 10, 30, 100, 300, 1000 and 3000 μM.

Time trace selection and HMM

Time traces from individual molecules were collected to measure polymerase binding times and to extract dwell times of open and closed fingers conformations. Because of variations

in the signal-to-noise ratio of molecules, as well as the presence of bleaching and blinking, an initial selection of molecules was made by hand; only DNA molecules that showed a constant *DD*+*DA* signal with sudden transitions (within 1 frame) from the free state to the bound state were selected. To determine the binding times, we first applied a 5-frame moving median filter to all selected traces, before applying additional selection criteria: 1) the sum of *DD* and *AA* is higher than 50 photons and 2) the FRET efficiency is higher than 0.4. Additionally, settings were such that the disappearance of donor signal (bleaching) was interpreted as the end of the trace and the disappearance of acceptor signal (bleaching or polymerase dissociation) was interpreted as the end of a binding event. The design of the experiment does not allow us to distinguish between acceptor bleaching and polymerase dissociation. Filtering traces following these criteria sometimes resulted in longer binding events being cut in multiple shorter events due to remaining noise. To prevent these cases, an exception was added to allow single-point excursions to lower intensities or FRET efficiencies. The final algorithm was found to identify most binding events that are also detectable by visual inspection. Extremely short events, however, were often not detected because of the median filter. These events may therefore be under-represented in our dwell time histograms.

In the end, this approach of data selection resulted in 30–50% of all identified single-molecule traces being used for later analysis. We consider this a good yield, since the remainder contains not only traces with misidentified events but also traces without any binding events at all and traces that are too noisy.

For extraction of fingers conformational changes, binding events from experiments with dTTPs were loaded into ebFRET, a software package for HMM (42). Because the final data point of some binding events may have a donor or acceptor that is already decreasing in intensity (just before the cutoff value that we set for dissociation or bleaching), we removed these points from the traces by applying a padding of 10 time points. Next, the prior for the minimal center position (open fingers) was set to $E^* = 0.4$ and that for the maximal center position (closed fingers) to $E^* = 0.8$. The convergence threshold was set to 10^{-5}.

Data availability

Raw data are available upon request. Please contact Johannes Hohlbein, Laboratory of Biophysics, Wageningen University & Research, Wageningen, 6708WE, The Netherlands; Tel: +31 317 482 635; Fax: +31 317 482 725; E-mail: johannes.hohlbein@wur.nl.

Acknowledgments—*E. coli* DNA Polymerase I (KF) was kindly supplied by Catherine Joyce, Timothy Craggs, and Achillefs Kapanidis.

Author contributions—C. F., M. M. M., M. K., R. K., M. F., J. B. T.-W., J. B. S., and J. H. data curation; C. F. software; C. F., M. M. M., M. K., R. K., M. F., J. B. T.-W., J. B. S., and J. H. formal analysis; C. F., M. M. M., M. K., R. K., M. F., J. B. T.-W., J. B. S., and J. H. methodology; C. F. writing-original draft; C. F., M. F. J. B. S., and J. H. writing-review and editing; M. M. M., J. B. T.-W., J. B. S., and J. H. conceptualization; J. B. S. and J. H. resources; J. B. S. and J. H. supervision; J. B. S. and J. H. funding acquisition.

Funding and additional information—This work was supported by a Marie Curie Career Integration Grant (Grant 630992 to J. H.). Funding for publication charges was from a Marie Curie Career Integration Grant.

Conflict of interest—The authors declare that they have no conflicts of interest with the contents of this article.

Abbreviations—The abbreviations used are: BER, base excision repair; Pol β, polymerase β; ALEX, alternating-laser excitation; TIRF, total internal reflection fluorescence; HMM, hidden Markov modelling.

References

1. Lindahl, T., and Wood, R. D. (1999) Quality control by DNA repair. *Science* **286,** 1897–1905 CrossRef Medline
2. Barnes, D. E., and Lindahl, T. (2004) Repair and genetic consequences of endogenous DNA base damage in mammalian cells. *Annu. Rev. Genet.* **38,** 445–476 CrossRef Medline
3. Bauer, N. C., Corbett, A. H., and Doetsch, P. W. (2015) The current state of eukaryotic DNA base damage and repair. *Nucleic Acids Res.* **43,** 10083–10101 CrossRef Medline
4. Dianov, G., and Lindahl, T. (1994) Reconstitution of the DNA base excision-repair pathway. *Curr. Biol.* **4,** 1069–1076 CrossRef Medline
5. Krokan, H. E., and Bjørås, M. (2013) Base excision repair. *Cold Spring Harb. Perspect. Biol.* **5,** a012583 CrossRef
6. Fromme, J. C., Banerjee, A., and Verdine, G. L. (2004) DNA glycosylase recognition and catalysis. *Curr. Opin. Struct. Biol.* **14,** 43–49 CrossRef Medline
7. Sobol, R. W., Horton, J. K., Kühn, R., Gu, H., Singhal, R. K., Prasad, R., Rajewsky, K., and Wilson, S. H. (1996) Requirement of mammalian DNA polymerase-β in base-excision repair. *Nature* **379,** 183–186 CrossRef Medline
8. Singhal, R. K., and Wilson, S. H. (1993) Short gap-filling synthesis by DNA polymerase beta is processive. *J. Biol. Chem.* **268,** 15906–15911
9. Yamtich, J., and Sweasy, J. B. (2010) DNA polymerase family X: function, structure, and cellular roles. *Biochim. Biophys. Acta* **1804,** 1136–1150 CrossRef Medline
10. Beard, W. A., and Wilson, S. H. (2014) Structure and mechanism of DNA polymerase β. *Biochemistry* **53,** 2768–2780 CrossRef Medline
11. Kim, S.-J., Lewis, M. S., Knutson, J. R., Porter, D. K., Kumar, A., and Wilson, S. H. (1994) Characterization of the tryptophan fluorescence and hydrodynamic properties of rat DNA polymerase β. *J. Mol. Biol.* **244,** 224–235 CrossRef Medline
12. Tang, K.-H., Niebuhr, M., Aulabaugh, A., and Tsai, M.-D. (2008) Solution structures of 2 :1 and 1 :1 DNA polymerase-DNA complexes probed by ultracentrifugation and small-angle X-ray scattering. *Nucleic Acids Res.* **36,** 849–860 CrossRef Medline
13. Sawaya, M. R., Prasad, R., Wilson, S. H., Kraut, J., and Pelletier, H. (1997) Crystal structures of human DNA polymerase β complexed with gapped and nicked DNA: evidence for an induced fit mechanism. *Biochemistry* **36,** 11205–11215 CrossRef Medline
14. Wu, E. Y., and Beese, L. S. (2011) The structure of a high fidelity DNA polymerase bound to a mismatched nucleotide reveals an "ajar" intermediate conformation in the nucleotide selection mechanism. *J. Biol. Chem.* **286,** 19758–19767 CrossRef Medline
15. Hohlbein, J., Aigrain, L., Craggs, T. D., Bermek, O., Potapova, O., Shoolizadeh, P., Grindley, N. D. F., Joyce, C. M., and Kapanidis, A. N. (2013) Conformational landscapes of DNA polymerase I and mutator derivatives

establish fidelity checkpoints for nucleotide insertion. *Nat. Commun.* **4,** 2131 CrossRef

16. Berezhna, S. Y., Gill, J. P., Lamichhane, R., and Millar, D. P. (2012) Single-molecule Förster resonance energy transfer reveals an innate fidelity checkpoint in DNA polymerase I. *J. Am. Chem. Soc.* **134,** 11261–11268 CrossRef Medline
17. Markiewicz, R. P., Vrtis, K. B., Rueda, D., and Romano, L. J. (2012) Single-molecule microscopy reveals new insights into nucleotide selection by DNA polymerase I. *Nucleic Acids Res.* **40,** 7975–7984 CrossRef Medline
18. Evans, G. W., Hohlbein, J., Craggs, T., Aigrain, L., and Kapanidis, A. N. (2015) Real-time single-molecule studies of the motions of DNA polymerase fingers illuminate DNA synthesis mechanisms. *Nucleic Acids Res.* **43,** 5998–6008 CrossRef Medline
19. Traut, T. W. (1994) Physiological concentrations of purines and pyrimidines. *Mol. Cell. Biochem.* **140,** 1–22 CrossRef Medline
20. Tang, K.-H., Niebuhr, M., Tung, C.-S., Chan, H., Chou, C.-C., and Tsai, M.-D. (2008) Mismatched dNTP incorporation by DNA polymerase β does not proceed via globally different conformational pathways. *Nucleic Acids Res.* **36,** 2948–2957 CrossRef Medline
21. Batra, V. K., Beard, W. A., Shock, D. D., Pedersen, L. C., and Wilson, S. H. (2008) Structures of DNA polymerase β with active-site mismatches suggest a transient abasic site intermediate during misincorporation. *Mol. Cell* **30,** 315–324 CrossRef Medline
22. Freudenthal, B. D., Beard, W. A., and Wilson, S. H. (2012) Structures of dNTP intermediate states during DNA polymerase active site assembly. *Structure* **20,** 1829–1837 CrossRef Medline
23. Freudenthal, B. D., Beard, W. A., Shock, D. D., and Wilson, S. H. (2013) Observing a DNA polymerase choose right from wrong. *Cell* **154,** 157–168 CrossRef Medline
24. Towle-Weicksel, J. B., Dalal, S., Sohl, C. D., Doublié, S., Anderson, K. S., and Sweasy, J. B. (2014) Fluorescence resonance energy transfer studies of DNA polymerase β: the critical role of fingers domain movements and a novel non-covalent step during nucleotide selection. *J. Biol. Chem.* **289,** 16541–16550 CrossRef Medline
25. Mahmoud, M. M., Schechter, A., Alnajjar, K. S., Huang, J., Towle-Weicksel, J., Eckenroth, B. E., Doublié, S., and Sweasy, J. B. (2017) Defective nucleotide release by DNA polymerase β mutator variant E288K is the basis of its low fidelity. *Biochemistry* **56,** 5550–5559 CrossRef Medline
26. Liptak, C., Mahmoud, M. M., Eckenroth, B. E., Moreno, M. V., East, K., Alnajjar, K. S., Huang, J., Towle-Weicksel, J. B., Doublié, S., Loria, J. P., and Sweasy, J. B. (2018) I260Q DNA polymerase β highlights precatalytic conformational rearrangements critical for fidelity. *Nucleic Acids Res.* **46,** 10740–10756 CrossRef Medline
27. Christian, T. D., Romano, L. J., and Rueda, D. (2009) Single-molecule measurements of synthesis by DNA polymerase with base-pair resolution. *Proc. Natl. Acad. Sci. U.S.A.* **106,** 21109–21114 CrossRef Medline
28. Hohlbein, J., Craggs, T. D., and Cordes, T. (2014) Alternating-laser excitation: single-molecule FRET and beyond. *Chem. Soc. Rev.* **43,** 1156–1171 CrossRef Medline
29. Hellenkamp, B., Schmid, S., Doroshenko, O., Opanasyuk, O., Kühnemuth, R., Rezaei Adariani, S., Ambrose, B., Aznauryan, M., Barth, A., Birkedal, V., Bowen, M. E., Chen, H., Cordes, T., Eilert, T., Fijen, C., *et al.* (2018) Precision and accuracy of single-molecule FRET measurements: a multi-laboratory benchmark study. *Nat. Methods* **15,** 669–676 CrossRef Medline
30. Craggs, T. D., Sustarsic, M., Plochowietz, A., Mosayebi, M., Kaju, H., Cuthbert, A., Hohlbein, J., Domicevica, L., Biggin, P. C., Doye, J. P. K., and Kapanidis, A. N. (2019) Substrate conformational dynamics facilitate structure-specific recognition of gapped DNA by DNA polymerase. *Nucleic Acids Res.* **47,** 10788–10800 CrossRef Medline
31. Kapanidis, A. N., Lee, N. K., Laurence, T. A., Doose, S., Margeat, E., and Weiss, S. (2004) Fluorescence-aided molecule sorting: analysis of structure and interactions by alternating-laser excitation of single molecules. *Proc. Natl. Acad. Sci. U.S.A.* **101,** 8936–8941 CrossRef Medline
32. Hwang, H., Kim, H., and Myong, S. (2011) Protein induced fluorescence enhancement as a single molecule assay with short distance sensitivity. *Proc. Natl. Acad. Sci. U.S.A.* **108,** 7414–7418 CrossRef Medline
33. Ploetz, E., Lerner, E., Husada, F., Roelfs, M., Chung, S., Hohlbein, J., Weiss, S., and Cordes, T. (2016) Förster resonance energy transfer and protein-induced fluorescence enhancement as synergetic multi-scale molecular rulers. *Sci. Rep.* **6,** 33257 CrossRef
34. Vande Berg, B. J., Beard, W. A., and Wilson, S. H. (2001) DNA structure and aspartate 276 influence nucleotide binding to human DNA polymerase β: implication for the identity of the rate-limiting conformational change. *J. Biol. Chem.* **276,** 3408–3416 CrossRef Medline
35. Kellinger, M. W., and Johnson, K. A. (2010) Nucleotide-dependent conformational change governs specificity and analog discrimination by HIV reverse transcriptase. *Proc. Natl. Acad. Sci. U.S.A.* **107,** 7734–7739 CrossRef Medline
36. Fijen, C., Montón Silva, A., Hochkoeppler, A., and Hohlbein, J. (2017) A single-molecule FRET sensor for monitoring DNA synthesis in real time. *Phys. Chem. Chem. Phys.* **19,** 4222–4230 CrossRef Medline
37. van Dijk, M., and Bonvin, A. M. J. J. (2009) 3D-DART: a DNA structure modelling server. *Nucleic Acids Res.* **37,** Suppl. 2, W235–W239 CrossRef Medline
38. Kalinin, S., Peulen, T., Sindbert, S., Rothwell, P. J., Berger, S., Restle, T., Goody, R. S., Gohlke, H., and Seidel, C. A. M. (2012) A toolkit and benchmark study for FRET-restrained high-precision structural modeling. *Nat. Methods* **9,** 1218–1225 CrossRef Medline
39. Farooq, S., and Hohlbein, J. (2015) Camera-based single-molecule FRET detection with improved time resolution. *Phys. Chem. Chem. Phys.* **17,** 27862–27872 CrossRef Medline
40. Cordes, T., Vogelsang, J., and Tinnefeld, P. (2009) On the mechanism of Trolox as antiblinking and antibleaching reagent. *J. Am. Chem. Soc.* **131,** 5018–5019 CrossRef Medline
41. Rasnik, I., McKinney, S. A., and Ha, T. (2006) Nonblinking and long-lasting single-molecule fluorescence imaging. *Nat. Methods* **3,** 891–893 CrossRef Medline
42. van de Meent, J.-W., Bronson, J. E., Wiggins, C. H., and Gonzalez, R. L., Jr. (2014) Empirical Bayes methods enable advanced population-level analyses of single-molecule FRET experiments. *Biophys. J.* **106,** 1327–1337 CrossRef Medline